RESEARCH ARTICLE

Mathematical Analysis and Parameter Estimation of a Two-Patch Zika Model

Kifah Al-Maqrashi[a], Fatma Al-Musalhi[b], Ibrahim Elmojtaba[a], Nasser Al-Salti[c]

[a]Department of Mathematics, Sultan Qaboos University, Muscat, Oman; [b]Centre of Preparatory Studies, Sultan Qaboos University, Muscat, Oman; [c]Department of Applied Mathematics and Science, National University of Science and Technology, Muscat, Oman

ABSTRACT

In this paper, we developed a multi-patch model for the spread of Zika virus infection taking, into account direct and indirect transmissions along with vertical transmission. The model was analyzed to gain insights into the disease's spread. The model was fitted to a data set collected from two neighboring countries, Brazil and Colombia, to estimate some of its parameters and use it for calculating $\Re_0$ and sensitivity analysis. Our results show that $\Re_0$ is less than one in both countries, which indicates that the disease will die out. Also, our results show that direct transmission is the most important route for spreading the disease; hence, it has to gain more focus in any controlling strategy.

1 Introduction

Zika virus is a virus of the genus *Flavivirus*, a member of the *Flaviviridae* family (Sherly and Bock, 2022; Wiratsudakul et al., 2018). In 1947, researchers were studying yellow fever in the forests of Uganda and identified the Zika virus in *rhesus* monkeys (Wiratsudakul et al., 2018). The first Zika virus outbreak outside of Africa and Asia was discovered in April 2007 on the island of Yap. The highest outbreak of Zika infection was reported in French Polynesia in 2013–2014, with an estimated 30,000 cases (Goswami et al., 2018). Following the commencement of an outbreak in Brazil in May 2015, the Zika virus has gained worldwide interest. Five months later, the Zika virus outbreak began in Colombia (Mattar et al., 2017). Since then, nearly 500,000 cases have been documented in more than 40 countries and territories (Maxian et al., 2017). Zika virus is transmitted through bites of *Aedes* female mosquitoes, which are typically found in Tropical and subtropical areas (Wiratsudakul et al., 2018). In 2008, it was discovered that the Zika virus has the potential for sexual (direct) transmission, which has never been seen before with other arboviruses (Agusto et al., 2017). In (Towers et al., 2016), based on the data from Colombia in 2015/2016, modelling analysis estimates that up to 47% of Zika virus cases were due to sexual contact.

Aside from these transmission routes, the virus can be transmitted vertically from a female to her infants in both mosquitoes and humans (Biswas et al., 2020; Bonyah et al., 2017). Zika-related deaths are uncommon; many people infected with the Zika virus have no symptoms or have mild symptoms that last a few days to a week, like rash, joint pain, and conjunctivitis (Cruz-Pacheco et al., 2019). It is estimated that approximately 80% of those infected with Zika are asymptomatic (Moreno et al., 2017). There is no definitive treatment for the Zika virus except controlling vectors with an insecticide spray, destroying larval breeding habitats (Bonyah et al., 2017) and slowing down or even stopping human movement or travel to affected areas.

The persistence of human mobility through distinct communities (patches or nodes) in a meta-community is an essential aspect to include in mathematical models of Zika disease because humans' mobility enhances both direct and indirect transmission, and it has the potential to accelerate the spread of the infection in the population. In order to describe the impacts of mobility in epidemiology, there have been two different approaches in the literature, namely the Lagrangian and the Eulerian approaches. Without explicitly simulating the flux of individuals, the Lagrangian technique tracks the effect of visits. This technique is more natural since it simulates short-term repeating motion patterns. On the other hand, the Eulerian approach illustrates actual people flux (Velázquez-Castro et al., 2018).

Different scientists and studies discussed the multi-patch mathematical models. In particular, Bichara and Castillo-Chavez (2016) discussed a mathematical model of a vector-borne disease via a general SI framework to account for vector dynamics

and an SIS framework to account for host dynamics to better understand the impact of host mobility on disease dynamics. A Lagrangian framework is used to explain host dispersal. Multi-group of the SEIR epidemic model where infectivity may depend on infection age is presented in the work of Bajiya et al. (2021). Velázquez-Castro et al. (2018) proposed a model of a meta-population framework using a Lagrangian approach to account for human intra-urban movement. They focus on two transmission indexes that influence infection spreading caused by: human behaviour and the particular spatial distribution of mosquitoes. Bonyah et al. (2017) construct a mathematical model for the Zika virus where the human population is divided into four sub-classes while the mosquito population is divided into three sub-classes. They incorporate time-dependent optimal controls, such as bed nets, pesticide treatment, and insecticide spraying. Furthermore, Velázquez-Castro et al. (2018) developed and analyzed a multi-fold Zika virus model. They considered overall Zika virus transmission in the adult and infants populations, separately through direct and indirect transmission routes.

In this paper, a two-patch vector-host mathematical model of the Zika virus is constructed to investigate the human movement's effect on disease transmission between nearby cities. This was a case study of Brazil and Colombia, where the model was fitted to real data, and some of its parameters were estimated. The rest of the paper is organized as follows: the model's building is presented in Section 2, and Section 3 contains some basic mathematical properties of the model. Next, the case study is presented in Section 4. Finally, we conclude our work in Section 5.

2   Model Formulation and Equations

To build our model, we consider the dynamics of the disease in a population involving two patches, where both hosts and vectors are included in each patch and connected by human movement. Vector's mobility across patches is ignored in our model as mosquitoes do not commonly travel long distances for a blood meal (Agusto et al., 2017; Russell et al., 2005). Because of this mobility, both direct and indirect transmissions occur at the same time, and the disease spreads across cities' borders. We limit our study to the case where the model (1) incorporates the state-dependence residence function, which accounts for the prevalence of infected vectors in each patch. That is, individuals are appealing to travel or move to areas (patches) with fewer infected mosquitoes, and they avoid visiting places with a high number of infectious mosquitoes. In each Patch i, the dynamic of the host populations is described by a SIR scheme with susceptible S_{hi}, infected I_{hi} and recovered R_{hi}. The susceptible individuals are recruited (died) through birth (death) at the per-capita rate μ_H, and they recover from infection at the per-capita rate γ_{hi}. The vectors' populations follow the SI framework with susceptible, S_{vi} and infected, I_{vi}. Both the host and vector populations are considered to be constant, i.e. $S_{hi} + I_{hi} + R_{hi} = N_{hi}$ and $S_{vi} + I_{vi} = N_{vi}$ such that N_{hi} and N_{vi} denote the total host and vector populations of Patch i for $i = 1, 2$, respectively. In humans, vertical transmission of the Zika virus has been confirmed; it was anticipated to pose 47% (Ades et al., 2021). In addition, the Zika virus has been reported in field-collected, larvae (5.49%), pupae (5.00%) and adult mosquitoes (6.99%), implying that Zika virus can be transmitted vertically in mosquitoes (Lai et al., 2020). Zika virus is assumed to spread by mosquitoes' bites in two types of host-vector interactions: susceptible mosquitoes (S_{vi}) may engage with infected humans (I_{hi}) at a rate of β_{hvi}, and infected mosquitoes (I_{vi}) may interact with susceptible humans (S_{hi}) at a rate of β_{vhi}. Note that the risk of infection β in Patch i differs by the patch to reflect spatial differences in potential infectivity (Bichara et al., 2015). Recent research has revealed that the Zika virus can be spread by vectors and sexual intercourse, as reported in 2016 (Biswas et al., 2020). Moreover, Zika virus transmission occurs when a susceptible and infectious individual in each sub-population i comes into adequate contact at a rate of β_{hhi}. We assume that the mobility pattern between the two patches is mostly Lagrangian (Bichara et al., 2015) (i.e., temporary movement rather than permanent migration) such that individuals in Patch i residents spend on average $p_{ij} \in [0, 1]$ time in Patch j with $\sum_{i=1}^{j=2} p_{ij} = 1$. A residence times matrix $P = [p_{ij}]_{1 \leqslant i,j \leqslant n} \in R_+^{2 \times 2}$ is used to track host-residence status and movements across patches, where p_{ij} is the fraction of time residents of Patch i spend in Patch j. This contact brings its own epidemiological dynamics, including being infected by or infecting members of their patch or the other patch and how much time members spend in their own patch or in the other patch (Lee et al., 2020). As a result, the incidence rate at which individuals from Patch i for $i = 1, 2$, residents in Patch j for $j = 1, 2$, become infected weighted by the host's interactions in each patch given by

$$\left(\overbrace{\beta_{hh1} p_{11} \left(\frac{p_{11} I_{h1} + p_{21} I_{h2}}{p_{11} N_{h_1} + p_{21} N_{h_2}} \right)}^{\text{in Patch 1}} + \overbrace{\beta_{hh2} p_{12} \left(\frac{p_{12} I_{h1} + p_{22} I_{h2}}{p_{12} N_{h_1} + p_{22} N_{h_2}} \right)}^{\text{in Patch 2}} \right) S_{h_1}$$

and

$$\left(\overbrace{\beta_{hh1} p_{21} \left(\frac{p_{11} I_{h1} + p_{21} I_{h2}}{p_{11} N_{h_1} + p_{21} N_{h_2}} \right)}^{\text{in Patch 1}} + \overbrace{\beta_{hh2} p_{22} \left(\frac{p_{12} I_{h1} + p_{22} I_{h2}}{p_{12} N_{h_1} + p_{22} N_{h_2}} \right)}^{\text{in Patch 2}} \right) S_{h_2}.$$
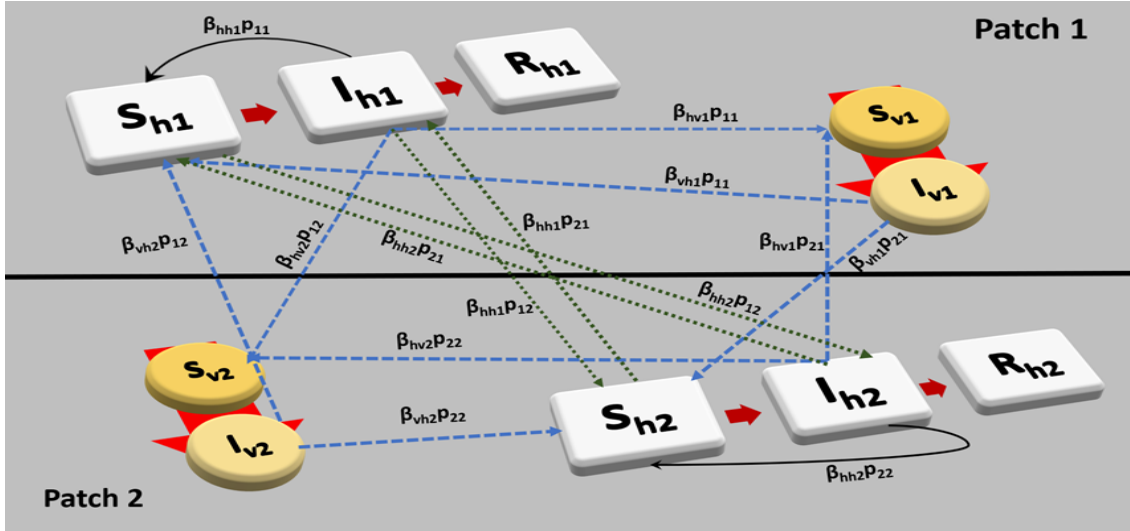
Figure 1: Flow chart of the proposed model (1).

Additionally, the number of newly infected Patch i for $i = 1, 2$, residents throughout their stay in Patch j for $j = 1, 2$, weighted by host-vector interaction in each patch is calculated as follows:

$$\left(\overbrace{\frac{\beta_{vh1}p_{11}I_{v_1}}{p_{11}N_{h_1} + p_{21}N_{h_2}}}^{\text{in Patch 1}} + \overbrace{\frac{\beta_{vh2}p_{12}I_{v_2}}{p_{12}N_{h_1} + p_{22}N_{h_2}}}^{\text{in Patch 2}}\right)S_{h_1} \quad \text{and} \quad \left(\overbrace{\frac{\beta_{vh1}p_{21}I_{v_1}}{p_{11}N_{h_1} + p_{21}N_{h_2}}}^{\text{in Patch 1}} + \overbrace{\frac{\beta_{vh2}p_{22}I_{v_2}}{p_{12}N_{h_1} + p_{22}N_{h_2}}}^{\text{in Patch 2}}\right)S_{h_2},$$

where, as long as there is a k such that $p_{kj} > 0$, resulting in a nonzero population in the Patch j, the $\sum_{k=1}^{2} N_k p_{kj}$ represents the total effective population of Patch j such that $\sum_{k=1}^{2} p_{kj}I_k$ are infected. Therefore, $\dfrac{\sum_{k=1}^{2} p_{kj}I_k}{\sum_{k=1}^{2} N_k p_{kj}}$ denotes the proportion of infected individuals in Patch j. This effective population of Patch j reflects the population's temporal dynamics in Patch j weighted by each group's mobility patterns and epidemiological state. The dynamic of the model is described in Figure 1.

When these assumptions are applied, the following set of nonlinear differential equations emerges:

$$
\begin{aligned}
S'_{h_1} &= \mu_H N_{h_1} - \mu_H \varepsilon_1 I_{h_1} - \left(\lambda_{vh_1} + \lambda_{hh_1}\right)S_{h_1} - \mu_H S_{h_1} & S'_{h_2} &= \mu_H N_{h_2} - \mu_H \varepsilon_2 I_{h_2} - \left(\lambda_{vh_2} + \lambda_{hh_2}\right)S_{h_2} - \mu_H S_{h_2} \\
I'_{h_1} &= \mu_H \varepsilon_1 I_{h_1} + \left(\lambda_{vh_1} + \lambda_{hh_1}\right)S_{h_1} - (\gamma_{h_1} + \mu_H)I_{h_1} & I'_{h_2} &= \mu_H \varepsilon_2 I_{h_2} + \left(\lambda_{vh_2} + \lambda_{hh_2}\right)S_{h_2} - (\gamma_{h_2} + \mu_H)I_{h_2} \\
R'_{h_1} &= \gamma_{h_1} I_{h_1} - \mu_H R_{h_1} & R'_{h_2} &= \gamma_{h_2} I_{h_2} - \mu_H R_{h_2} \\
S'_{v_1} &= \mu_V N_{v_1} - \mu_V \varepsilon_3 I_{v_1} - \lambda_{hv_1} S_{v_1} - \mu_V S_{v_1} & S'_{v_2} &= \mu_V N_{v_2} - \mu_V \varepsilon_4 I_{v_2} - \lambda_{hv_2} S_{v_2} - \mu_V S_{v_2} \\
I'_{v_1} &= \mu_V \varepsilon_3 I_{v_1} + \lambda_{hv_1} S_{v_1} - \mu_V I_{v_1} & I'_{v_2} &= \mu_V \varepsilon_4 I_{v_2} + \lambda_{hv_2} S_{v_2} - \mu_V I_{v_2}
\end{aligned}
\tag{1}
$$

such that

$$\lambda_{vh_1} = \frac{\beta_{vh1}p_{11}I_{v_1}}{p_{11}N_{h_1} + p_{21}N_{h_2}} + \frac{\beta_{vh2}p_{12}I_{v_2}}{p_{12}N_{h_1} + p_{22}N_{h_2}}, \qquad \lambda_{vh_2} = \frac{\beta_{vh1}p_{21}I_{v_1}}{p_{11}N_{h_1} + p_{21}N_{h_2}} + \frac{\beta_{vh2}p_{22}I_{v_2}}{p_{12}N_{h_1} + p_{22}N_{h_2}},$$

$$\lambda_{hv_1} = \beta_{hv1}\left(\frac{p_{11}I_{h_1} + p_{21}I_{h_2}}{p_{11}N_{h_1} + p_{21}N_{h_2}}\right), \qquad \lambda_{hv_2} = \beta_{hv2}\left(\frac{p_{12}I_{h_1} + p_{22}I_{h_2}}{p_{12}N_{h_1} + p_{22}N_{h_2}}\right),$$

$$\lambda_{hh_1} = \beta_{hh1}p_{11}\left(\frac{p_{11}I_{h1} + p_{21}I_{h2}}{p_{11}N_{h_1} + p_{21}N_{h_2}}\right) + \beta_{hh2}p_{12}\left(\frac{p_{12}I_{h1} + p_{22}I_{h2}}{p_{12}N_{h_1} + p_{22}N_{h_2}}\right),$$

$$\lambda_{hh_2} = \beta_{hh1}p_{21}\left(\frac{p_{11}I_{h1} + p_{21}I_{h2}}{p_{11}N_{h_1} + p_{21}N_{h_2}}\right) + \beta_{hh2}p_{22}\left(\frac{p_{12}I_{h1} + p_{22}I_{h2}}{p_{12}N_{h_1} + p_{22}N_{h_2}}\right),$$

subjected to non-negative initial conditions

$$\left(S_{h_1}(0), I_{h_1}(0), R_{h_1}(0), S_{v_1}(0), I_{v_1}(0), S_{h_2}(0), I_{h_2}(0), R_{h_2}(0), S_{v_2}(0), I_{v_2}(0)\right)^T, \tag{2}$$

Table 1: Description of constant paramters in model (1) constant parameters for $i, j = 1, 2$.

Symbol	Description
μ_H	Natural birth/death rate of humans
μ_V	Natural birth/death rate of mosquitoes
β_{vhi}	Disease risk during the interaction of infected mosquitoes with susceptible humans in Patch i
β_{hvi}	Disease risk during the interaction of susceptible mosquitoes with infected humans in Patch i
β_{hhi}	Disease risk during the interaction between humans in Patch i
γ_{h_i}	The recovery rate of human population in Patch i
$\varepsilon_1, \varepsilon_2$	Probability of vertical transmission in humans in Patch i, respectively
$\varepsilon_3, \varepsilon_4$	Probability of vertical transmission in mosquitoes in Patch i, respectively
p_{ij}	Time proportion spent by an individual of Patch i in Patch j

and where

$$N_{h_i} = S_{h_i}(t) + I_{h_i}(t) + R_{h_i}(t) \quad \text{and} \quad N_{v_i} = S_{v_i}(t) + I_{v_i}(t) \quad \text{for} \quad i = 1, 2. \tag{3}$$

The parameter descriptions for model (1) are given in Table 1.

2.1   State-dependent residence rime function

Generally, people avoid locations with a high prevalence of vectors, or spend less time in them; this human behaviour is captured by imposing natural constraints on P entries so that the time fraction spent in a given patch is dependent on the number of infected vectors present in that patch. Hence, we define

$$\Bbbk_{ij} := \Bbbk_{i,j}(I_{v1}, I_{v2}) \quad \text{for} \quad i, j = 1, 2,$$

to be the proportion of time a resident of Patch i spends in Patch j owing to the presence of infectious mosquitoes. We assume that people living in a patch with a high number of infected vectors may choose to travel to a patch with fewer infected vectors and they are less likely to travel to a patch with a high number of infectious mosquitoes. When $i \neq j$, that fraction may have attributes such as a rise about the growth of infected vectors in patch i (I_{vi}) or a reduction about infected vectors in patch j (I_{vj}) such that

$$\frac{\partial k_{12}(I_{v1}, I_{v2})}{\partial I_{v1}} \geqslant 0, \quad \frac{\partial k_{12}(I_{v1}, I_{v2})}{\partial I_{v2}} \leqslant 0, \quad \text{and} \quad \frac{\partial k_{21}(I_{v1}, I_{v2})}{\partial I_{v1}} \geqslant 0, \quad \frac{\partial k_{21}(I_{v1}, I_{v2})}{\partial I_{v2}} \leqslant 0. \tag{4}$$

These inequalities can be minimized by utilizing the relation $k_{ij}(I_{v1}, I_{v2}) + k_{ji}(I_{v1}, I_{v2}) = 1$, to

$$\frac{\partial k_{11}(I_{v1}, I_{v2})}{\partial I_{v1}} \leqslant 0 \quad \text{and} \quad \frac{\partial k_{22}(I_{v1}, I_{v2})}{\partial I_{v2}} \leqslant 0. \tag{5}$$

The following functions can be used to represent such dependencies that guarantee the desired behaviour responses (Bichara et al., 2015) that are described in relations (4):

$$k_{ii}(I_{vi}, I_{vj}) = \frac{\delta_{ii} + \delta_{ii}I_{vi} + I_{vj}}{1 + I_{vi} + I_{vj}} \quad \text{and} \quad k_{ij}(I_{vi}, I_{vj}) = \delta_{ij} \frac{1 + I_{vi}}{1 + I_{vi} + I_{vj}}, \tag{6}$$

where $(i, j) \in 1, 2$ and $\delta_{ij} = p_{ij}(0, 0)$ with $\sum_{j=1}^{2} \delta_{ij} = 1$. In the proposed two-patch system (1), the function's forms are

$$k_{11}(I_{v1}, I_{v2}) = \frac{\delta_{11} + \delta_{11}I_{v1} + I_{v2}}{1 + I_{v1} + I_{v2}}, \qquad\qquad k_{22}(I_{v1}, I_{v2}) = \frac{\delta_{22} + \delta_{22}I_{v2} + I_{v1}}{1 + I_{v1} + I_{v2}},$$

$$k_{12}(I_{v1}, I_{v2}) = \delta_{12} \frac{1 + I_{v1}}{1 + I_{v1} + I_{v2}}, \qquad\qquad k_{21}(I_{v1}, I_{v2}) = \delta_{21} \frac{1 + I_{v2}}{1 + I_{v1} + I_{v2}},$$

such that $\delta_{11} + \delta_{12} = 1$ and $\delta_{22} + \delta_{21} = 1$.

If there is no disease in both patches or one disease-free patch, the fraction of time an individual spends in their patch is nonzero in the state-dependent situation. Therefore, the following work is done by considering the state-dependent residence functions $\Bbbk$ for the proposed meta-patch Zika model (1).

3 Basic Reproduction Number $\mathfrak{R}_0$

Introduce that the effective density of infected individuals in Patch j is given by

$$\ell_j := \delta_{1j} N_{h1} + \delta_{2j} N_{h2}, \quad \text{for} \quad j = 1, 2.$$

Model (1) possesses a unique disease-free equilibrium (*DFE*), provided by χ^0 in the absence of infected hosts and infected vectors in all patches. That is

$$\chi^0 := \left(S_{h_1}^0, 0, 0, S_{v_1}^0, 0, S_{h_2}^0, 0, 0, S_{v_2}^0, 0 \right)^T,$$

where $S_{h_i}^0 = N_{hi}, S_{v_i}^0 = N_{vi}$ for $i = 1, 2$. The basic reproduction number is the average number of secondary cases created by an infected individual throughout its lifetime (Bichara and Castillo-Chavez, 2016). This threshold quantity for the meta-population model (1), indicated by $\mathfrak{R}_0$, will be computed using the next-generation operator approach (Van den Driessche and Watmough, 2002). The right-hand side of the system (1) could be written as $\mathcal{M} + \mathcal{N}$, where $\mathcal{M}$ is the matrix of new infection terms in the infected compartments of the model (1) and $\mathcal{N}$ is the associated matrix of linear transition terms in the infected compartments of the model (1). Let $M := D\mathcal{M}$, evaluated at the *DFE* : χ^0 such that

$$M = \begin{bmatrix} \left(\frac{\beta_{hh1} \delta_{11}^2}{\ell_1} + \frac{\beta_{hh2} \delta_{12}^2}{\ell_2} \right) N_{h1} & \frac{\beta_{vh1} \delta_{11} N_{h1}}{\ell_1} & \left(\frac{\beta_{hh1} \delta_{11} \delta_{21}}{\ell_1} + \frac{\beta_{hh2} \delta_{12} \delta_{22}}{\ell_2} \right) N_{h1} & \frac{\beta_{vh2} \delta_{12} N_{h1}}{\ell_2} \\ \frac{\beta_{hv1} \delta_{11} N_{v1}}{\ell_1} & 0 & \frac{\beta_{hv1} \delta_{21} N_{v1}}{\ell_1} & 0 \\ \left(\frac{\beta_{hh1} \delta_{11} \delta_{21}}{\ell_1} + \frac{\beta_{hh2} \delta_{22} \delta_{12}}{\ell_2} \right) N_{h2} & \frac{\beta_{vh1} \delta_{21} N_{h2}}{\ell_1} & \left(\frac{\beta_{hh1} \delta_{21}^2}{\ell_1} + \frac{\beta_{hh2} \delta_{22}^2}{\ell_2} \right) N_{h2} & \frac{\beta_{vh2} \delta_{22} N_{h2}}{\ell_2} \\ \frac{\beta_{hv2} \delta_{12} N_{v2}}{\ell_2} & 0 & \frac{\beta_{hv2} \delta_{22} N_{v2}}{\ell_2} & 0 \end{bmatrix},$$

and $N := D\mathcal{N}$, evaluated at the *DFE* : χ^0 such that

$$N = \begin{bmatrix} \mu_H(1 - \varepsilon_1) + \gamma_{h1} & 0 & 0 & 0 \\ 0 & \mu_V(1 - \varepsilon_3) & 0 & 0 \\ 0 & 0 & \mu_H(1 - \varepsilon_2) + \gamma_{h2} & 0 \\ 0 & 0 & 0 & \mu_V(1 - \varepsilon_4) \end{bmatrix},$$

then the related next generation matrix MN^{-1} is

$$\begin{bmatrix} \frac{\left(\frac{\beta_{hh1} \delta_{11}^2}{\ell_1} + \frac{\beta_{hh2} \delta_{12}^2}{\ell_2} \right) N_{h1}}{\mu_H(1 - \varepsilon_1) + \gamma_{h1}} & \frac{\beta_{vh1} \delta_{11} N_{h1}}{\mu_V(1 - \varepsilon_3)\ell_1} & \frac{\left(\frac{\beta_{hh1} \delta_{11} \delta_{21}}{\ell_1} + \frac{\beta_{hh2} \delta_{12} \delta_{22}}{\ell_2} \right) N_{h1}}{\mu_H(1 - \varepsilon_2) + \gamma_{h2}} & \frac{\beta_{vh2} \delta_{12} N_{h1}}{\mu_V(1 - \varepsilon_4)\ell_2} \\ \frac{\beta_{hv1} \delta_{11} N_{v1}}{\left(\mu_H(1 - \varepsilon_1) + \gamma_{h1} \right)\ell_1} & 0 & \frac{\beta_{hv1} \delta_{21} N_{v1}}{\left(\mu_H(1 - \varepsilon_2) + \gamma_{h2} \right)\ell_1} & 0 \\ \frac{\left(\frac{\beta_{hh1} \delta_{11} \delta_{21}}{\ell_1} + \frac{\beta_{hh2} \delta_{22} \delta_{12}}{\ell_2} \right) N_{h2}}{\mu_H(1 - \varepsilon_1) + \gamma_{h1}} & \frac{\beta_{vh1} \delta_{21} N_{h2}}{\mu_V(1 - \varepsilon_3)\ell_1} & \frac{\left(\frac{\beta_{hh1} \delta_{21}^2}{\ell_1} + \frac{\beta_{hh2} \delta_{22}^2}{\ell_2} \right) N_{h2}}{\mu_H(1 - \varepsilon_2) + \gamma_{h2}} & \frac{\beta_{vh2} \delta_{22} N_{h2}}{\mu_V(1 - \varepsilon_4)\ell_2} \\ \frac{\beta_{hv2} \delta_{12} N_{v2}}{\left(\mu_H(1 - \varepsilon_1) + \gamma_{h1} \right)\ell_2} & 0 & \frac{\beta_{hv2} \delta_{22} N_{v2}}{\left(\mu_H(1 - \varepsilon_2) + \gamma_{h2} \right)\ell_2} & 0 \end{bmatrix}. \tag{7}$$

The basic reproduction number $\mathfrak{R}_0$ is the spectral radius of the next generation matrix:

$$\mathfrak{R}_0 := \rho \left(MN^{-1} \right). \tag{8}$$

A closed form of the basic reproduction number $\mathfrak{R}_0$ can be calculated using symbolic math programs. However, because of the magnitude of our model, it is too complicated and lengthy to be presented here. Hence, $\mathfrak{R}_0$ will be calculated numerically in later sections by substituting the values of the parameters in the next generation matrix and then calculating the spectral radius of the matrix.

Note that since it is computed in an infection-free state χ^0, the basic reproduction number $\mathfrak{R}_0$ is the same as if we use irreducible (constant) residence time matrix P instead of $\Bbbk$ (Bichara et al., 2015). Moreover, if $\mathfrak{R}_0 > 1$, the infection will continue to spread throughout all patches, and if $\mathfrak{R}_0 < 1$, the infection will die out in both patches. Hence, the value of $\mathfrak{R}_0$ determines the local stability of the unique equilibrium χ^0. So, according to (Bichara et al., 2015; Van den Driessche and Watmough, 2002), we can establish the following theorem:

Theorem 1. *If $\mathfrak{R}_0 < 1$, the DFE: given by χ^0, is locally asymptotically stable. However, if $\mathfrak{R}_0 > 1$, it is unstable.*

4   A Case Study of Brazil and Colombia

It has been established that human movement may extend Zika virus transmission risk to a broader demographic. Black et al. (2019) suggested that Zika virus infections were likely imported into Colombia throughout the epidemic, which indicates that the movement between Brazil and Colombia may be the most critical drive in the emergence of the Zika virus in Colombia. In this section, we will apply our model to the two neighboring countries, Brazil and Colombia, to estimate the model's parameters, calculate $\mathfrak{R}_0$, and carry out some sensitivity analysis of $\mathfrak{R}_0$ to the model's parameters.

4.1   Curve fitting and parameter estimation

In 2015, the Zika virus expanded rapidly in South American countries, particularly Brazil and Colombia, as reported by PAHO/WHO (WHO, 2016). Colombia was the second Latin American country, after Brazil, that experienced many cases of the Zika virus epidemic in 2015 (Black et al., 2019). According to the case report in (Mattar et al., 2017), the first reported case of maternal Zika virus in Colombia was comparable to those previously seen in Brazil between 2015 and 2016. In Brazil, the Zika virus was found in 14 states, and in Colombia, out of 98 samples, nine were confirmed to be ZIKV positive. More than 6000 Zika-virus-infected individuals were reported in Brazil between October 2015 and February 2016, including 139 cases of congenital microcephaly. Between December 2015 and February 2016, almost 200 Guillain-Barré Syndrome cases were identified in Colombia, possibly related to Zika infection (Goswami et al., 2018). Moreover, as announced in (Statisa, 2022), Colombia reported 69 cases in 2022, and 94 cases of Zika virus disease in 2021, down from 165 infections the previous year. In addition, Brazil reported approximately 17.5 thousand cases of Zika virus disease in 2021, down from nearly 19 thousand infections the previous year. With over 200 thousand cases in Brazil and over 91 thousand cases in Colombia, in this study we use the data of 2016; this year was the most Zika infections cases in the South American country.

The proposed model (1) will now be fitted to weekly cumulative infected individuals data from the two countries, Brazil and Colombia, reported by PAHO/WHO (PAHO, 2022). The weekly confirmed cases for the time interval of 53 weeks from 1st week of January 2016 to the last week of December 2016 are shown in Figure 2. For each fitting, the optimization function in Matlab **fminsearchbnd** will be used to find the optimal values for the unknown parameters of our model. The **fminsearchbnd** function is applied to minimize the sum of squares of errors (**SSE**) between the cumulative data of confirmed cases and the number of cumulative infected of the model for varying parameters. To improve the fitting, we set the lower and upper bounds for each parameter depending on the estimation of those parameters as found in the literature. Let the subscripts b and c denote the patch residents for Brazil (Patch 1) and Colombia (Patch 2), respectively. It should be noted that the fundamental model (1) has 20 parameters, ten of which are known from the literature or assumed to have some constant values as ($\mu_H, \mu_V, \varepsilon_1, \varepsilon_2, \varepsilon_3$ and ε_4) and they are given in Table 2. The values of the total population sizes are also shown in Table 2. The remaining parameters ($\beta_{hvb}, \beta_{hvc}, \beta_{vhb}, \beta_{vhc}, \beta_{hhb}, \beta_{hhc}, \gamma_{h_b}, \gamma_{h_c}, \delta_{bc}$ and δ_{cb}) are estimated by running the model (1) with cumulative infected individuals of Zika virus for Brazil and Colombia. First, we fit model (1) by taking into consideration the state-dependent (reducible) residences function $\Bbbk$. The fitting of the weekly cumulative cases of both countries is displayed in Figure 3. The estimated parameters are given in Table 3.

Moreover, the parameters ($\beta_{hvb}, \beta_{hvc}, \beta_{vhb}, \beta_{vhc}, \beta_{hhb}, \beta_{hhc}, \gamma_{h_b}, \gamma_{h_c}, p_{bc}$ and p_{cb}) are estimated again by running the model (1) with cumulative infected individuals with Zika data for Brazil and Colombia. This time we consider the time-independent (irreducible) residence matrix P. Figure 5 illustrates the model output against the weekly cumulative Zika infection data for Brazil and Colombia, respectively. Table 4 tabulates the estimated values of the unknown parameters obtained. Numerical simulations of infected humans and vectors in the two patches are given in Figures 4, and 6. In Figure 4 with the state-dependent residence matrix $\Bbbk$, we note that the peak time of infected humans of both patches is almost the same. However, in Figure 6 with time-independent residence function P, the peak time of the number of infected humans in Patch 1 happens more quickly compared with the peak of Patch 1. Moreover, in Figures, 4 and 6, the number of infected in Patch 2 reaches its steady state faster than in Patch 1.

Figure 7 shows the number of infected humans for the state-dependent and independent cases in both patches. For the state-dependent case, it is clear that the maximum number of infected is much lower than the number of infected in the time-independent case in both patches. In Patch 1, the number of infected cases in state-dependent cases decreases faster than in time-independent cases. While in Patch 2 the time-independent case is much faster than the state-dependent case. For the graphs of

Figure 2: Weekly number of cases for Brazil and Colombia, respectively in 2016.

Table 2: Values for fixed parameters.

Parameter	Value	Unit	Source
N_{h_b}	209568×10^3	p.(week)$^{-1}$	PAHO, 2022
N_{h_c}	48654×10^3	p.(week)$^{-1}$	PAHO, 2022
N_{v_b}	6×10^5	m.(week)$^{-1}$	assumed
N_{v_c}	3×10^4	m.(week)$^{-1}$	assumed
μ_H	$1/60$	(year)$^{-1}$	assumed
μ_V	$1/14$	(day)$^{-1}$	Bonyah and Okosun, 2016
$\varepsilon_1, \varepsilon_2$	0.5	—	Ades et al., 2021
$\varepsilon_3, \varepsilon_4$	0.06	—	Lai et al., 2020

Table 3: Estimated parameters for model (1) with the state-dependent residence matrix for Brazil and Colombia (per week).

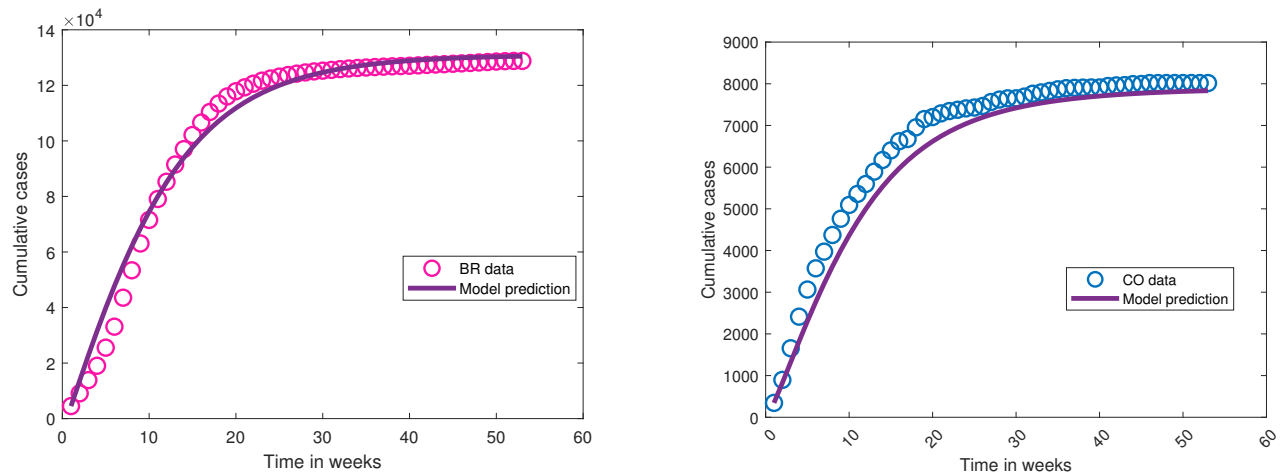| Parameter	β_{hv_b}	β_{vh_b}	β_{hh_b}	γ_{h_b}	δ_{bb}	β_{hv_c}	β_{vh_c}	β_{hh_c}	γ_{h_c}	δ_{cc}
Value	2.9567	0.0586	2.4768	2.000	0.7028	0.0660	0.0031	0.5867	0.9386	0.8378

Figure 3: The solutions of model (1) with P matrix fitted with weekly cumulative infected individuals of Zika virus for 53 weeks in Brazil and Colombia, respectively.

Table 4: Estimated parameters for model (1) with the time-independent residence matrix for Brazil and Colombia (per week).

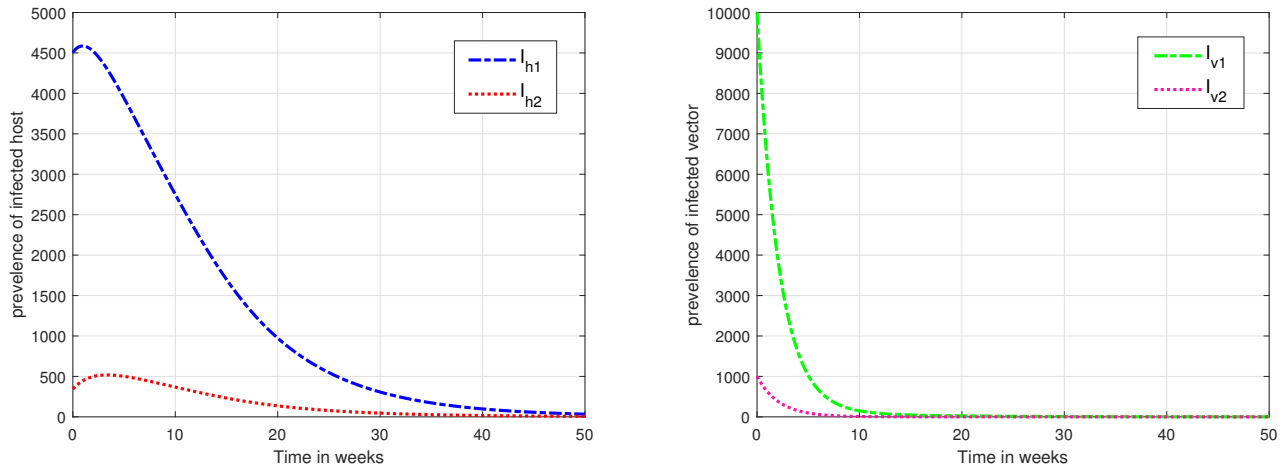| Parameter	β_{hv_b}	β_{vh_b}	β_{hh_b}	γ_{h_b}	p_{bb}	β_{hv_c}	β_{vh_c}	β_{hh_c}	γ_{h_c}	p_{cc}
Value	0.001	0.1189	1.5527	1.2060	0.7	0.0193	3.000	0.1793	1.4327	0.9490

Figure 4: Time series of the point prevalence of infected host and infected vector in two patches (countries), connected according to the $\Bbbk$-time residence matrix, displaying fixed and fitted parameters of the proposed model (1) described in Tables 2 and 3.
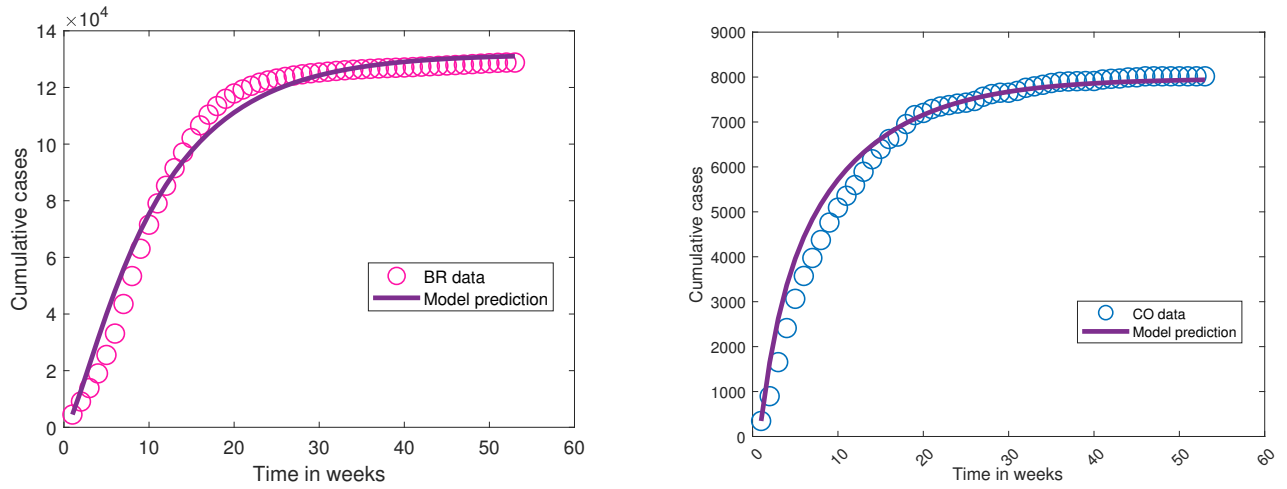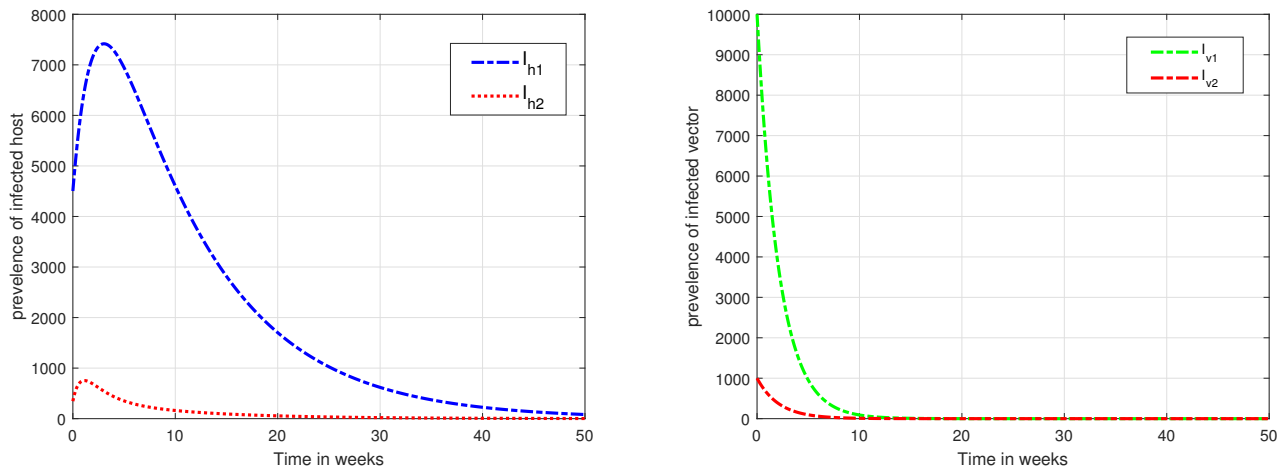

Figure 5: The solutions of model (1) with $\Bbbk$ matrix fitted with weekly cumulative infected individuals of Zika virus for 53 weeks in Brazil and Colombia, respectively.

Figure 6: Time series of the point prevalence of infected host and infected vector in two patches (countries), connected according to the P-time residence matrix, displaying fixed and fitted parameters of the proposed model (1) described in Tables 2 and 4.
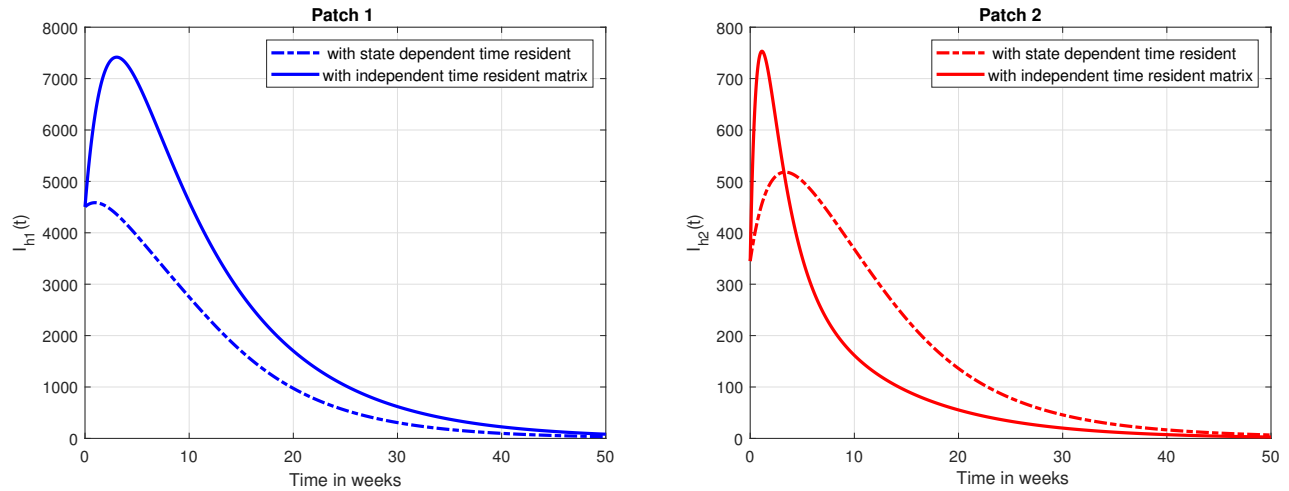
Figure 7: Time series of the point prevalence of infected host in two patches (Brazil and Colombia) of the proposed model (1) according to different time-mobility matrices using fixed and estimated constant parameters in Tables 2–4.

model (1) with a state-dependent residence matrix, the movement of humans depends on the number of infected vectors in a given patch. In contrast, for model (1) graphs with a time-independent residence matrix, the time spent by individuals in a given patch is constant. Therefore, the overall prevalence in both patches depends on human mobility and behaviour.

4.2   Numerical calculation of $\mathfrak{R}_0$

It is important to note here that the calculation of the basic reproduction number $\mathfrak{R}_0$ depends on the estimated parameters of the model. Here, the basic reproduction number $\mathfrak{R}_0$ will be calculated numerically by directly substituting the values of related parameters given in Table 2 and Table 3 in the corresponding next generation matrix (MN^{-1}), given by (7), and then calculating the eigenvalues of the matrix. Let us denote the reproduction number of Brazil by $\mathfrak{R}_{0b}$, and the reproduction number of Colombia by $\mathfrak{R}_{0c}$. Furthermore, $\mathfrak{R}_0$ is the spectral radius of the matrix (MN^{-1}):

$$\mathfrak{R}_0 := \max\{\mathfrak{R}_{0b}, \mathfrak{R}_{0c}\}. \tag{9}$$

Additionally, when the state-dependent function $\Bbbk$ connects the two patches (countries), we find that the reproduction number for Brazil $\mathfrak{R}_{0b}$ is around 0.9574, and the reproduction number for Colombia $\mathfrak{R}_{0c}$ is around 0.1508. As a result, in comparison to its neighbour, Colombia, Brazil had more disease risk. However, $\mathfrak{R}_0 = 0.9574$ is below one ($\mathfrak{R}_0 < 1$), which indicates that the Zika virus in both countries will eventually die out.

Similarly, when the two patches (countries) are connected by time-independent matrix P, we find that the reproduction number for Brazil $\mathfrak{R}_{0b}$ is around 0.91666 and Colombia's reproduction number $\mathfrak{R}_{0c}$ is calculated to be 0.04658. Hence, our calculations of basic reproduction numbers of both countries were below one ($\mathfrak{R}_0 < 1$), indicating that the disease will die out.

4.3   Sensitivity analysis

In this section, a global sensitivity analysis is used to analyze the influence of uncertainty and the sensitivity of the numerical simulation results to alterations in each parameter of the proposed model. The Latin Hypercube Sampling-Partial Rank Correlation Coefficient (LHS-PRCC) sensitivity analysis procedure has been carried out to evaluate the most sensitive parameters in the investigation of efficient disease control methods. LHS is a so-called stratified sampling without replacement technique, which assumes that the sampling is performed independently for each parameter. PRCC assesses the strength of the link between the model's outcome and the parameters, indicating the magnitude of each parameter's influence on the outcome. PRCC values vary between −1 and 1, indicating perfect negative and positive correlations, respectively. The magnitude of PRCC shows the parameter significance, while the sign of PRCC gives the direction of the relationship between the input parameter and the model output. A negative PRCC value indicates that as the parameter value increases, the value of the model output decreases. In contrast, a positive value means that as the parameter value increases, the value of the model output increases. Moreover, the identification of the relative significance of each of the parameters is verified using p-values (probability value). The parameters that have the most significant impact on the model are those corresponding with small p-values ($p < 0.05$) and large magnitude PRCC values ($0.5 < |PRCC| < 1$).
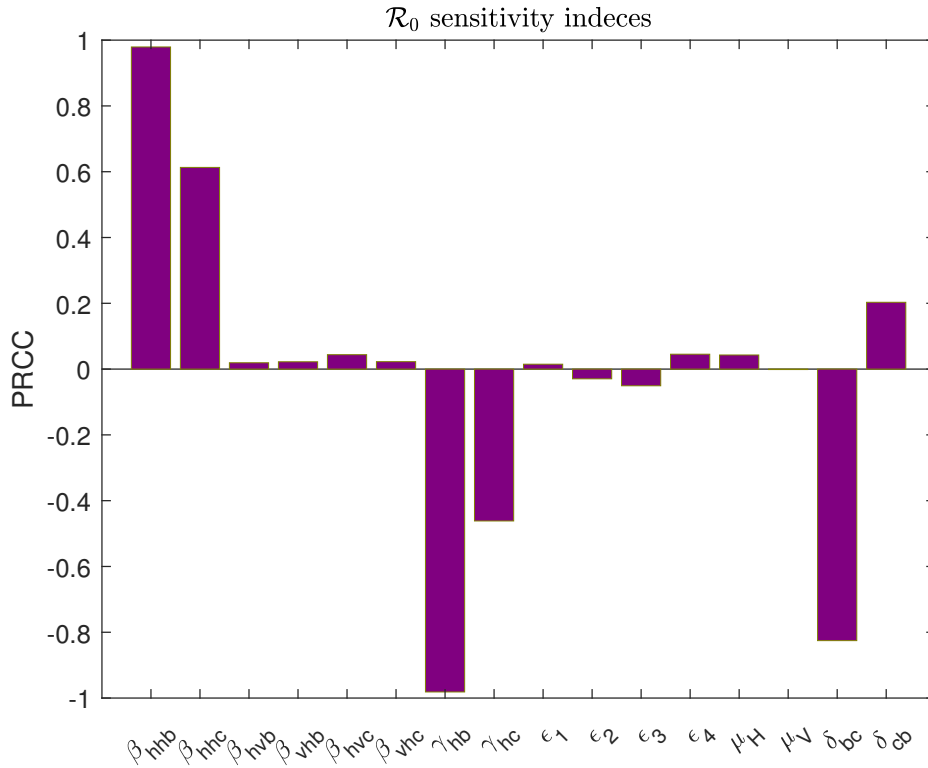
Figure 8: Global sensitivity for model (1) parameters with state-dependent function $\Bbbk$, using parameter values in Tables 2 and 3 and the reproduction number $\mathcal{R}_0$ as response functions, through LHS/PRCC scheme with 95% confidence interval.

By using the baseline values listed in Table 2 and Table 3, with the response function of basic reproduction number $\mathcal{R}_0$, we assume all model parameters are uniformly distributed while generating the LHS matrices. The LHS matrix is created, with N rows for the number of simulations (sample size) and k columns for the number of different parameters. The models were then subjected to 1000 simulations for each LHS run.

Figure 8 carries out the global sensitivity analysis PRCC of the model (1) to see how changing model parameters affected the number of cases. According to our finding, as the model is subjected to state-dependent matrix $\Bbbk$ and 95% confidence interval, the system's basic reproduction number varies as $\mathcal{R}_{0b} = [0.9095, 1.0052]$, $\mathcal{R}_{0c} = [0.1432, 0.1583]$ and therefore $\mathcal{R}_0 > 1$. Hence, the most critical positive influence parameters in the spread of Zika infection are the disease risk during the interaction between humans in both patches, in Brazil β_{hhb} and Colombia β_{hhc} and the time proportion spent by the individual from Brazil in Colombia δ_{cb}. Thus, the prevalence of the disease increases (decreases) as they increase (decrease). On the other hand, the human recovery rate in both patches γ_{hb} and γ_{hc} and the time proportion spent by individuals from Colombia in Brazil δ_{bc} significantly adversely affect on the reproduction number $\mathcal{R}_0$. Thus, the prevalence of the disease increases (decreases) as they decrease (increase). Note that δ_{cb} and δ_{bc} have opposite sign sensitivity indices, since residents through continuous human movement from the high-risk Patch (Brazil) to the lower-risk Patch (Colombia), and the inverse will be effective in curtailing or spreading of Zika virus infection between patches. Using the baseline values listed in Table 2 and Table 4 with the response function of basic reproduction number $\mathcal{R}_0$. Figure 9 carries out the global sensitivity analysis PRCC of the model (1), as the model subjected to constant time-independent matrix P and 95% confidence interval, the system basic reproduction number varies as $\mathcal{R}_{0b} = [0.8708, 0.9625]$, $\mathcal{R}_{0c} = [0.04426, 0.0489]$ and therefore $\mathcal{R}_0 < 1$. Hence, the most critical positive influence parameters in the spread of Zika virus infection are the disease risk during the interaction between humans in both patches, in Brazil β_{hhb} and Colombia β_{hhc}. On the other hand, the human recovery rate in both patches γ_{hb} and γ_{hc} and the time proportion spent by individuals from Colombia in Brazil δ_{bc} significantly adversely affect on the reproduction number $\mathcal{R}_0$. Note that p_{cb} and p_{bc} have negative sensitivity indices; they have a negative impact on the influence of the disease. Since the system is in a disease-free state in both patches, the increase in the time residents through continuous human movement from the high-risk Patch (Brazil) to the lower-risk Patch (Colombia) will have a lower effect on the spreading of ZIKV infection between patches. In both cases (P and $\Bbbk$), p-values of the parameters, that are not significant using the PRCC approach are greater than 0.05, and their variations have a negligible impact on the reproduction number $\mathcal{R}_0$ either positively or negatively, as is clearly shown in Figure 10.
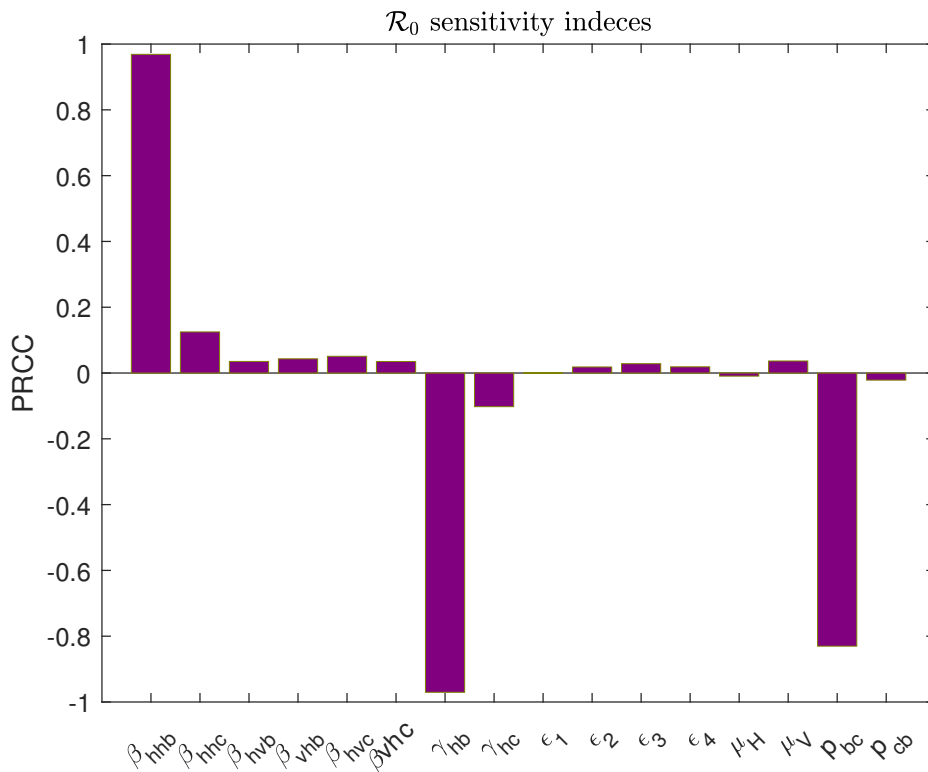
Figure 9: Global sensitivity for model (1) parameters of with constant time-independent matrix P, using parameter values in Tables 2 and 4 and the reproduction number $\mathcal{R}_0$ as response functions, through LHS/PRCC scheme with 95% confidence interval.
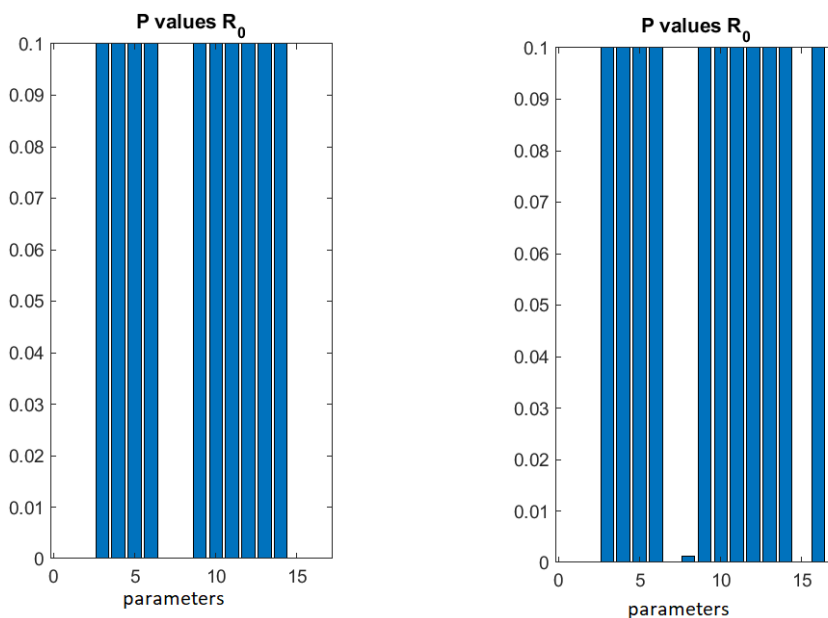

Figure 10: p-values of the estimated parameters for dependent and independent residents cases, receptively.

5   Conclusions

A vector-host meta-population model of Zika virus disease has been developed including human direct and vertical transmissions and indirect transmission through mosquito bites. Human mobility between patches has been considered state-dependent residence function $\Bbbk$. The model was analyzed to see how human travel from one patch to another affects Zika virus transmission over time. A case study of the movement between Brazil and Colombia was taken into account, where the model's parameters were estimated from the data of Brazil and Colombia. Our results show that the basic reproduction number for Brazil is greater than the basic reproduction number for Colombia, and both are less than one which suggests that the disease will be eradicated from both countries eventually. Our sensitivity analysis shows that the direct transmission of the disease has the most positive impact on the spread of the disease in both patches, which suggests that the best control strategy is to use protection in any sexual activity. Our results also show that when the system is in the endemic state, the time spent in each patch has a significant impact on the spread of the disease, whereas when the system is in a disease-free state, this time has a lower impact.

References

Ades, A., A. Soriano-Arandes, A. Alarcon, F. Bonfante, C. Thorne, C. S. Peckham, and C. Giaquinto (2021). Vertical transmission of zika virus and its outcomes: a bayesian synthesis of prospective studies. *The Lancet Infectious Diseases 21*(4), 537–545. 30, 35

Agusto, F., S. Bewick, and W. Fagan (2017). Mathematical model for zika virus dynamics with sexual transmission route. *Ecological Complexity 29*, 61–81. 29, 30

Bajiya, V. P., J. P. Tripathi, V. Kakkar, J. Wang, and G. Sun (2021). Global dynamics of a multi-group seir epidemic model with infection age. *Chinese Annals of Mathematics, Series B 42*(6), 833–860. 30

Bichara, D. and C. Castillo-Chavez (2016). Vector-borne diseases models with residence times–a lagrangian perspective. *Mathematical biosciences 281*, 128–138. 29, 33

Bichara, D., Y. Kang, C. Castillo-Chavez, R. Horan, and C. Perrings (2015). Sis and sir epidemic models under virtual dispersal. *Bulletin of mathematical biology 77*(11), 2004–2034. 30, 32, 34

Biswas, S. K., U. Ghosh, and S. Sarkar (2020). Mathematical model of zika virus dynamics with vector control and sensitivity analysis. *Infectious Disease Modelling 5*, 23–41. 29, 30

Black, A., L. H. Moncla, K. Laiton-Donato, B. Potter, L. Pardo, A. Rico, C. Tovar, D. P. Rojas, I. M. Longini, M. E. Halloran, et al. (2019). Genomic epidemiology supports multiple introductions and cryptic transmission of zika virus in colombia. *BMC infectious diseases 19*(1), 1–11. 34

Bonyah, E., M. A. Khan, K. Okosun, and S. Islam (2017). A theoretical model for zika virus transmission. *PloS one 12*(10), e0185540. 29, 30

Bonyah, E. and K. O. Okosun (2016). Mathematical modeling of zika virus. *Asian Pacific Journal of Tropical Disease 6*(9), 673–679. 35

Cruz-Pacheco, G., L. Esteva, and C. P. Ferreira (2019). A mathematical analysis of zika virus epidemic in rio de janeiro as a vector-borne and sexually transmitted disease. *Journal of Biological Systems 27*(01), 83–105. 29

Goswami, N. K., A. K. Srivastav, M. Ghosh, and B. Shanmukha (2018). Mathematical modeling of zika virus disease with nonlinear incidence and optimal control. In *Journal of Physics: Conference Series*, Volume 1000, pp. 012114. IOP Publishing. 29, 34

Lai, Z., T. Zhou, J. Zhou, S. Liu, Y. Xu, J. Gu, G. Yan, and X.-G. Chen (2020). Vertical transmission of zika virus in aedes albopictus. *PLoS neglected tropical diseases 14*(10), e0008776. 30, 35

Lee, S., O. Baek, and L. Melara (2020). Resource allocation in two-patch epidemic model with state-dependent dispersal behaviors using optimal control. *Processes 8*(9), 1087. 30

Mattar, S., C. Ojeda, J. Arboleda, G. Arrieta, I. Bosch, I. Botia, N. Alvis-Guzman, C. Perez-Yepes, L. Gerhke, and G. Montero (2017). Case report: microcephaly associated with zika virus infection, colombia. *BMC infectious diseases 17*(1), 1–4. 29, 34

Maxian, O., A. Neufeld, E. J. Talis, L. M. Childs, and J. C. Blackwood (2017). Zika virus dynamics: When does sexual transmission matter? *Epidemics 21*, 48–55. 29

Moreno, V. M., B. Espinoza, D. Bichara, S. A. Holechek, and C. Castillo-Chavez (2017). Role of short-term dispersal on the dynamics of zika virus in an extreme idealized environment. *Infectious Disease Modelling 2*(1), 21–34. 29

PAHO (2022). Health information platforms for the americas(plisa),data reported by health ministries of the countries. `https://www3.paho.org/data/index.php/en/mnu-topics/zika-weekly-en/`. 34, 35

Russell, R. C., C. Webb, C. Williams, and S. Ritchie (2005). Mark–release–recapture study to measure dispersal of the mosquito aedes aegypti in cairns, queensland, australia. *Medical and veterinary entomology 19*(4), 451–457. 30

Sherly, A. and W. Bock (2022). Multipatch zikv model and simulations. In *European Consortium for Mathematics in Industry*, pp. 433–438. Springer. 29

Statisa (2022). Number of reported zika virus disease cases in colombia from 2015 to 2022. `https://www.statista.com/statistics/1006902/colombia-zika-virus-cases/`. 34

Towers, S., F. Brauer, C. Castillo-Chavez, A. K. Falconar, A. Mubayi, and C. M. Romero-Vivas (2016). Estimate of the reproduction number of the 2015 zika virus outbreak in barranquilla, colombia, and estimation of the relative role of sexual transmission. *Epidemics 17*, 50–55. 29

Van den Driessche, P. and J. Watmough (2002). Reproduction numbers and sub-threshold endemic equilibria for compartmental models of disease transmission. *Mathematical biosciences 180*(1-2), 29–48. 33, 34

Velázquez-Castro, J., A. Anzo-Hernández, B. Bonilla-Capilla, M. Soto-Bajo, and A. Fraguela-Collar (2018). Vector-borne disease risk indexes in spatially structured populations. *PLoS neglected tropical diseases 12*(2), e0006234. 29, 30

WHO (2016). World health organization (who), who statement on the first meeting of the international health regulations (2005) emergency committee on zika virus and observed increase in neurological disorder sandneo natalmal for mations. `https://www.who.int/news/item/01-02-2016-who-statement-on-the-first-meeting-of-the-international-health-regulations-(2005)-(ihr-2005)-emergency-committee-on-zika-virus-and-observed-increase-in-neurological-disorders-and-neonatal-malformations`. 34

Wiratsudakul, A., P. Suparit, and C. Modchang (2018). Dynamics of zika virus outbreaks: an overview of mathematical modeling approaches. *PeerJ 6*, e4526. 29